Magnetic properties of a quasi-one-dimensional $S=1/2$ antiferromagnet: Copper benzoate

D. C. Dender, D. Davidović, Daniel H. Reich, and Collin Broholm*
Department of Physics and Astronomy, The Johns Hopkins University, Baltimore, Maryland 21218

Kim Lefmann
Department of Solid State Physics, Risø National Laboratory, DK-4000 Roskilde, Denmark

G. Aeppli†
AT&T Bell Laboratories, Murray Hill, New Jersey 07974
(Received 23 August 1995)

We use magnetic susceptibility and inelastic neutron scattering measurements to show that copper benzoate, $Cu(C_6D_5COO)_2\cdot 3D_2O$, is a quasi-one-dimensional $S=1/2$ antiferromagnet with an exchange constant $J=1.57$ meV. Below $T=0.8$ K a ferromagnetic contribution to the susceptibility marks the onset of canted three-dimensional (3D) antiferromagnetic order. An external magnetic field suppresses this effect, and the susceptibility measured in high field shows only the response of a $S=1/2$ chain. The dynamic correlation function $\mathcal{S}(\tilde{q},\omega)$ measured by neutron scattering shows only 1D spin correlations for $\hbar\omega \geqslant 0.4$ meV at $T=1.8$ K. There is clear evidence of a continuum of magnetic excitations, consistent with the current theoretical picture of the excitation spectrum of the $S=1/2$ chain at $T=0$ K.

I. INTRODUCTION

The linear chain $S=1/2$ Heisenberg antiferromagnet (AFM) is of fundamental importance in many-body physics, as it is one of the few systems where a nontrivial ground state is known exactly.[1] This ground state has only quasi-long-range order with power law decay of the instantaneous spin correlations.[2] The Hamiltonian for this system in an applied magnetic field $\mathbf{H}$ is

$$\mathscr{H}=\sum_i \left[J\mathbf{S}_i\cdot\mathbf{S}_{i+1}-g\mu_B\mathbf{H}\cdot\mathbf{S}_i\right]. \tag{1}$$

Unlike spin-wave excitations in ordered magnets, which are spin-1 objects, the elementary excitations of the $S=1/2$ chain, known as spinons, carry spin 1/2.[3] Although the spinons have a well-defined dispersion relation, they can be produced only in pairs, and the resulting magnetic excitation spectrum of the continuum bounded from below by the des Cloiseaux–Pearson (dCP) relation[4]

$$\epsilon_1(\tilde{q})=\frac{\pi}{2}J|\sin\tilde{q}| \tag{2}$$

and above by

$$\epsilon_2(\tilde{q})=\pi J|\sin(\tilde{q}/2)|. \tag{3}$$

There is now considerable theoretical and numerical evidence for this continuum based on Bethe ansatz, exact diagonalization, and quantum Monte Carlo studies.[5–10] The $\pi/2$ enhancement of $\epsilon_1(\tilde{q})$ compared to spin-wave theory was first observed experimentally by inelastic neutron scattering experiments on the material CPC.[11] Hints of the continuum were found in line shape asymmetries observed in CPC (Ref. 12) and $KCuF_3$,[13,14] but the best evidence to date comes from recent experiments on $KCuF_3$ that show a clear magnetic response at energies well above the dCP lower bound.[15,16]

There remain, however, a number of important questions that deserve further study. These include the dynamics in high magnetic fields,[6,17,18] and the proximity of the system to a $T=0$ quantum critical point.[19] It is thus of interest to obtain and characterize additional $S=1/2$ materials to address these issues. In this work, we present magnetic susceptibility and inelastic neutron scattering measurements on copper benzoate that demonstrate that it is a clean model system that is particularly well suited for magnetic field studies. We have also obtained a complete mapping of the spinon continuum for this material.

II. EXPERIMENT

Copper benzoate, $Cu(C_6H_5COO)_2\cdot 3H_2O$, was identified as a linear chain antiferromagnet by Date *et al.*[20] Its crystal structure is monoclinic with room temperature lattice constants $a=6.98$ Å, $b=34.12$ Å, $c=6.30$ Å, and $\beta=89.5°$.[21] At $T=4.2$ K, we find $a=6.913$ Å, $c=6.225$ Å, and $\beta=89.3°$. The Cu^{2+} ions form chains along the c axis, with a Cu-Cu distance of $c/2$. There are two copper sites that alternate along the chain with local symmetry axes that differ by 20°.[20] This is relevant for the low-temperature and low-field properties as will be discussed below. Through Faraday balance, electron spin resonance (ESR), and NMR measurements Date *et al.* determined the exchange constant along the chain to be $J=1.5\pm0.1$ meV from a comparison to the standard Bonner-Fisher result for the susceptibility $\chi(T)$ of the $S=1/2$ AFM chain.[22] Substantial deviations from the Bonner-Fisher curve were reported for 4 K $<T<$ 8 K, particularly for $\mathbf{H}\|\hat{\mathbf{c}}$, where there was a sharp upturn in $\chi(T)$ at the lowest temperatures. No field dependence of χ was reported. We note that these techniques involve the application

 © 1996 The American Physical Society

of fields of order several kOe, and thus the low-field features we describe below were not observed. Spin diffusion in this material has been studied extensively by ESR and NMR,[23] and evidence has been reported for Néel ordering at $T_N = 0.76$ K.[24]

A. Sample preparation

Copper benzoate is insoluble in water, but single crystals may be grown from water solutions by a diffusion method.[20] The crystals grow as flat plates in the (010) plane with well-defined edges parallel to the c axis. To grow deuterated samples for neutron scattering studies, crystallization dishes with vertical glass dividers separating the reagents C_6D_5COONa and $CuSO_4 \cdot 5H_2O$ were slowly filled with D_2O under a N_2 atmosphere. The dishes were placed in sealed jars in a cold water bath at $T=10$ °C for 5–8 days while the crystals grew on the tops of the dividers. Typical crystal dimensions were $5\times0.4\times15$ mm^3 along the $\hat{\mathbf{a}}$, $\hat{\mathbf{b}}$, and $\hat{\mathbf{c}}$ axes, respectively. Deuteration was $>95\%$ as determined by prompt γ-ray neutron activation analysis.[25]

B. Susceptibility

We have performed a detailed exploration of the ac susceptibility $\chi(H,T)$ as a function of temperature and dc magnetic field. The susceptibilities measured with the magnetic field parallel to the principal crystal axes are denoted χ^a, χ^b, and χ^c, respectively. For $3<T<300$ K, measurements were made in a commercial (Quantum Design) superconducting quantum interference device (SQUID) magnetometer. Below 8 K, measurements were made with a home-built ac susceptometer mounted on the top loader of a dilution refrigerator. To obtain sufficient sensitivity for these measurements, the pickup coils of the ac susceptometer were connected to a low-temperature LC circuit consisting of a superconducting inductor $L=0.1$ H in series with a capacitor $C\sim1$ μF. When the susceptometer is driven at $f_0=1/2\pi\sqrt{LC}\sim550$ Hz, the LC circuit provides both a highly stable gain of $Q=200$ and good matching to the noise figure contour of the room temperature lock-in detection electronics. At f_0, the sensitivity of the susceptometer is 2×10^{-10} emu/$\sqrt{\text{Hz}}$ in zero field. This sensitivity decreases by only a factor of 1.5 at $H=2$ T.

C. Neutron scattering

For inelastic neutron scattering measurements, the sample consisted of approximately 450 deuterated crystals arranged in six stacks. The crystals were aligned by placing their c-axis edges against a metal plate and clamping the stack. The total sample mass was 3.47 g, and the mosaic was 5° in the $(h0l)$ scattering plane. The Cu atoms in a chain are spaced by $\mathbf{c}/2$, and so we refer to momentum transfer along the chain as $\tilde{q}=\mathbf{Q}\cdot\mathbf{c}/2=l\pi$. The experiment was performed on the TAS7 cold neutron triple-axis spectrometer at Risø National Laboratory in Denmark. All measurements were made with the pyrolythic graphite PG(002) analyzer fixed at a nominal final energy $E_f = 5.1$ meV. Full width at half maximum (FWHM) beam divergences were $60'/k(\text{Å}^{-1})-49'$ around the PG(002) monochromator, k being the incident neutron wave vector and $100'-256'$ around the analyzer. A liquid-nitrogen-cooled beryllium filter was used after the sample to exclude neutrons with energies above 5.1 meV from the detection system. This filter also had the effect of transferring the good energy resolution of the monochromating system to the $\hbar\omega>0$ side of the overall energy resolution function of the instrument whose FWHM for incoherent elastic scattering was $\Delta E=0.23$ meV.

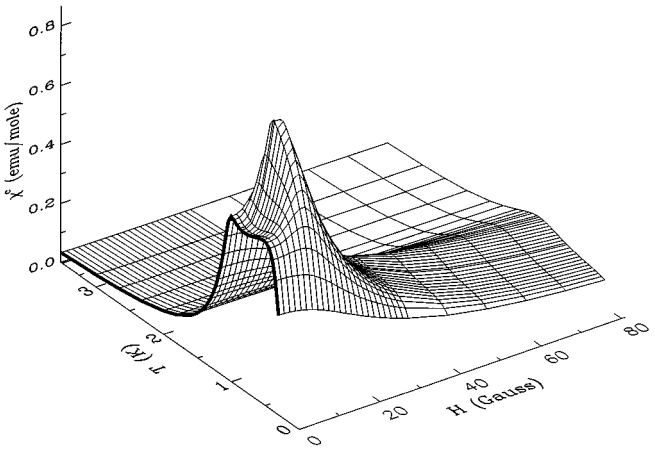

FIG. 1. ac susceptibility for $\mathbf{H}\parallel\hat{\mathbf{c}}$ of copper benzoate at low field. The intersections of the grid correspond to measured points. The bold curve highlights the zero-field response.

III. RESULTS AND DISCUSSION

A. Susceptibility

In copper benzoate in small fields, the magnetic response associated with linear chain antiferromagnetism is obscured by a large paramagnetic feature at low temperatures. As will be shown below, this feature is suppressed by the application of a magnetic field, and the one-dimensional (1D) behavior may be observed directly in the susceptibility for $H\geqslant 2$ T. At very low fields $H<50$ Oe, χ is highly anisotropic. χ^c is as much as 10 times bigger than χ^a and 100 times bigger than χ^b. This prevents accurate measurements of χ^b, as even a 1° misalignment between the ac field and $\hat{\mathbf{b}}$ is sufficient to cause a significant error. Figure 1 shows χ^c for $0.3\leqslant T\leqslant 3.5$ K and $H\leqslant 80$ Oe. This figure is a 3D representation of a data set containing approximately 1000 measured values of χ^c. The intersections of the lines on the grid correspond directly to the data points. The spacing between points in T is $\Delta T=0.05$ K for $0.3\leqslant T\leqslant 2$ K, and $\Delta T=0.3$ K for $T>2$ K. The spacing in H is $\Delta H=1.4$ Oe for $H\leqslant 32$ Oe and $\Delta H=10$ Oe for $H>32$ Oe. The zero-field susceptibility is indicated by a thick black line. Note that there is a sharp peak in χ^c at $T=0.8$ K and $H=20$ G. Above this field, χ^c is drastically reduced. At temperatures below the peak and for fields near the peak, the imaginary component of the susceptibility χ'' was nonzero. Coupled with the concomitant decrease in χ', this indicates that the average spin relaxation time grows larger than $1/2\pi f_0$ in this region. χ'' is negligible, however, for fields greater than 50 G.

The presence of two different orientations of the local environment of the Cu sites and the large susceptibility for $\mathbf{H}\parallel\hat{\mathbf{c}}$ suggests that spin canting occurs along that direction as

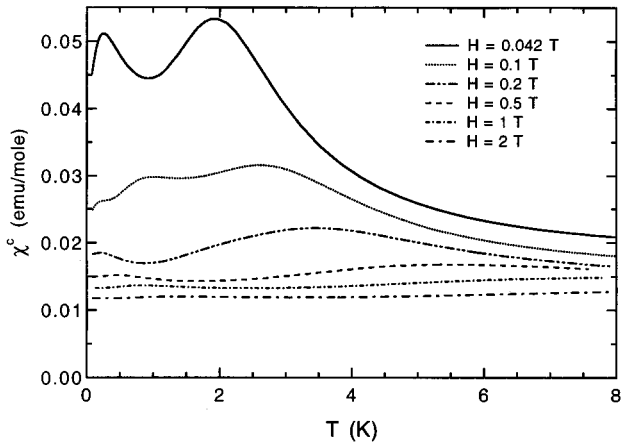

FIG. 2. ac susceptibility for $\mathbf{H}\|\hat{\mathbf{c}}$ of copper benzoate. Note suppression of low-field paramagnetic signal with increasing field.

the system enters a three-dimensional antiferromagnetically ordered state.[29] The small value of χ^b indicates that $\hat{\mathbf{b}}$ is the easy axis for the antiferromagnetic order. Similar ac susceptibilities of weak ferromagnets have been reported previously.[30] The observed long relaxation times at low fields can be attributed to the motion of domain walls. Applying a weak field is sufficient to align the domains, at which point the ac susceptibility is reduced and independent of frequency.

To further suppress the weak ferromagnetic response due to the spin canting, we measured $\chi(T)$ in progressively larger fields. Figure 2 shows the temperature dependence of χ^c as H is increased. As H increases, χ_c decreases further, and its temperature dependence changes. For $H \geqslant 1$ T, the susceptibility is an increasing function of temperature in the range of temperatures shown, and effects due to linear chain antiferromagnetism can be observed. This is demonstrated in Fig. 3, which shows the susceptibility measured with the

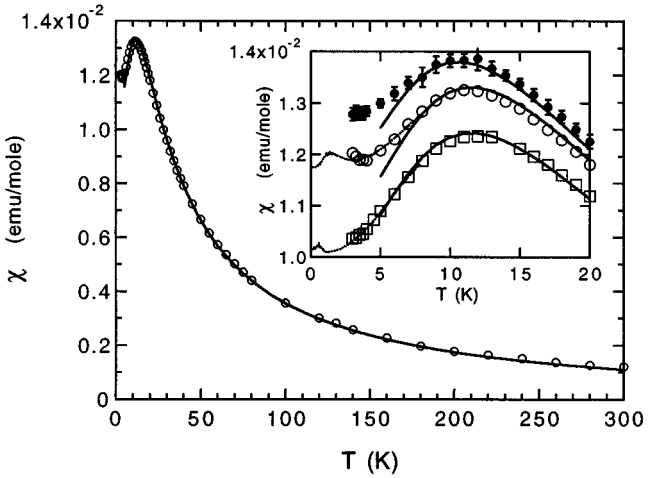

FIG. 3. High-field susceptibility of copper benzoate for $H = 2$ T $\|\hat{c}$. Inset: open squares, χ^a at $H = 2$ T; open circles, χ^c at $H = 2$ T; solid circles, χ^c at $H = 5$ T. Dashed lines: low temperature susceptibility χ^a and χ^c at $H = 2$ T. Solid lines: fit with $J = 1.57$ meV as described in the text.

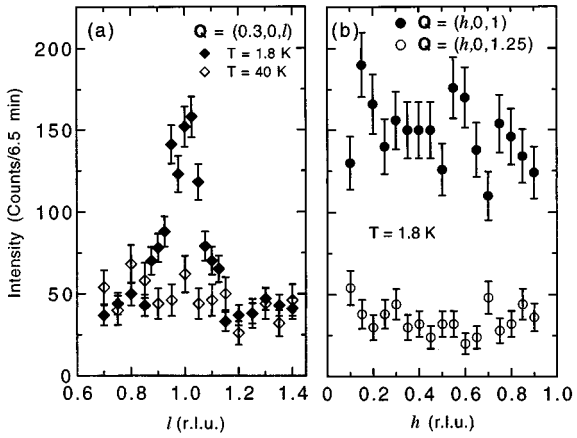

FIG. 4. Wave vector dependence of inelastic neutron scattering at $\hbar\omega = 0.4$ meV (a) for $\mathbf{Q} = (0.3,0,l)$ varying only along the chain direction at $T = 1.8$ K (solid symbols) and $T = 40$ K (open symbols), and (b) for $\mathbf{Q} = (h,0,1)$ and $\mathbf{Q} = (h,0,1.25)$ varying only perpendicular to the chain direction at $T = 1.8$ K.

SQUID at fields $H = 2$ T and 5 T $\|\hat{\mathbf{c}}$ and $H = 2$ T $\|\hat{\mathbf{a}}$. As can be seen in the inset, χ is much more isotropic than at low fields. The inset also shows the low-temperature data at $H = 2$ T, where the remnant of the low-field feature can still be seen. Note that low-temperature c-axis data at $H = 2$ T are the same curve as that in Fig. 2. The main part of Fig. 3 shows χ^c for $H = 2$ T over our full temperature range, and shows clearly the characteristic response of a 1D antiferromagnet.

To determine the parameters in $\mathscr{H}$ [Eq. (1)] appropriate for copper benzoate, we fit the data in Fig. 3 to $\chi(H,T)$ calculated from exact diagonalization of $\mathscr{H}$ for spin chains of up to 16 sites. Comparison between results for chains with even and odd numbers of spins indicates that $\chi(H,T)$ calculated in this manner is valid for $k_B T/J > 0.25$, and we therefore confined our fits to the temperature range $5 \leqslant T \leqslant 300$ K. Using $g_a = 2.17$ and $g_c = 2.27$, the values determined by ESR,[20] our three data sets with $H_a = 2$ T and $H_c = 2$ and 5 T were fit simultaneously, yielding $J = 1.57 \pm 0.01$ meV $(= k_B \times 18.2 \pm 0.1$ K). The results of this fit are shown as solid lines in Fig. 3, demonstrating that linear chain antiferromagnetism dominates the bulk properties of this material at high magnetic fields.

B. Neutron scattering

Inelastic neutron scattering provides additional proof that copper benzoate is a quasi-one-dimensional antiferromagnet. Figure 4 shows the $\mathbf{Q}$ dependence of the inelastic scattering intensity at $\hbar\omega = 0.4$ meV along lines parallel and perpendicular to the chain direction in the $(h0l)$ reciprocal lattice plane. Parallel to the chain direction, the intensity distribution is strongly peaked for $\mathbf{Q}\cdot\hat{\mathbf{c}} = c^*$, corresponding to wave vector transfer $\tilde{q} = \pi$ along the chain. Because this peak vanishes on warming to $T = 40$ K [open diamonds in Fig. 4(a)], it must arise from magnetic scattering and not scattering from phonons, which increases with temperature. From the position of the peak we conclude that spins displaced from each other by $\mathbf{c}/2$ are antiferromagnetically correlated. Figure

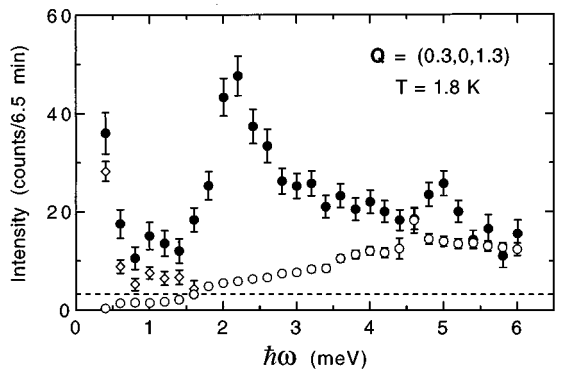

FIG. 5. Solid symbols show raw inelastic neutron scattering intensity versus energy for copper benzoate at $T = 1.8$ K and $\mathbf{Q} = (0.3,0,1.3)$ corresponding to $\tilde{q} = 1.3\pi$. The asymmetric peak at $\hbar\omega \approx 2$ meV is magnetic. The dashed line shows the average detector count rate after extracting the sample from the cryostat. Open symbols show the background contributions from incompletely resolved elastic nuclear scattering (diamonds) and from inelastic nuclear scattering (open circles) as determined by the procedures described in the text.

4(b) shows that there is no discernible variation of the inelastic scattering intensity with momentum transfer perpendicular to the chain whether the parallel component $\mathbf{Q}\cdot\hat{\mathbf{c}}$ corresponds to the center of the peak in Fig. 4(a) ($\tilde{q} = \pi$) or not ($\tilde{q} = 1.25\pi$). This proves that magnetic correlations are absent along $\hat{\mathbf{a}}$ for energies down to $\hbar\omega = 0.4$ meV. We have not probed the $\mathbf{Q}\cdot\hat{\mathbf{b}}$ dependence of the magnetic scattering, but since the spin chains are separated by 34 Å along $\hat{\mathbf{b}}$, any magnetic interactions must be even smaller along that direction than along $\hat{\mathbf{a}}$. Therefore, we conclude that magnetic correlations at $T = 1.8$ K are antiferromagnetic and purely one-dimensional in the energy range $\hbar\omega \geq 0.4$ meV probed by these neutron scattering measurements.

We now turn to a detailed investigation of the $\tilde{q}$ and ω dependence of the magnetic scattering cross section. Since the cross section is independent of $\mathbf{Q}\cdot\hat{\mathbf{a}}$, we can choose this component of wave vector transfer to optimize resolution and signal to noise. The broad sample mosaic ($\eta \approx 5°$ FWHM) makes the projection of the resolution function onto the direction in the horizontal plane perpendicular to $\mathbf{Q}$, $|\delta\mathbf{Q}_\perp| \approx 0.09|Q|$, longer than its projection onto $\mathbf{Q}$, $|\delta\mathbf{Q}_\parallel| \approx 0.04$ Å^{-1}. The best resolution of wave vector transfer along the chain, $\tilde{q}$, is therefore achieved for $\mathbf{Q} \| \hat{\mathbf{c}}$. However, to avoid background from a ridge of coherent diffuse elastic scattering along $\mathbf{Q} = (h01)$, we chose to perform the experiment along the $(0.3,0,l)$ direction. Data were taken at $T = 1.8$ K on a grid in the range $\pi \leq \tilde{q} \leq 2\pi$ and 0.4 meV $\leq \hbar\omega \leq$ 6 meV with grid spacings 0.1π and 0.2 meV, respectively.

Figure 5 shows a constant $\tilde{q} = 1.3\pi$ cut through the raw intensity distribution (solid circles). We observe an asymmetric peak with a lower bound of 1.75 meV and a high-energy tail that extends up to at least 4 meV. The low-energy upturn arises from incoherent elastic scattering. Although the magnetic signal is clearly visible, a detailed determination of the background, which we shall now describe, is necessary to establish the nature of the magnetic scattering cross section. After extracting the sample with its aluminum holder from the cryostat, we measured the contribution to the detector count rate not associated with neutrons scattered from the sample region. Under these conditions, the count rate throughout the range of $\mathbf{Q}$ and ω described above was 3.2(3) counts/10^7 monitor counts $\approx$ 6.5 min. This is shown as a dashed line in Fig. 5. Upon subtracting this constant background and applying a measured, $\hbar\omega$-dependent factor compensating for the contribution to the monitor count rate from higher order neutrons reflected by the monochromator, the magnetic contribution to the data is proportional to $|F(Q)|^2\tilde{I}(\tilde{q},\omega)$, where $F(Q)$ is the magnetic form factor[26] and

$$\tilde{I}(\mathbf{Q},\omega) = \frac{1}{2}\sum_{\alpha\beta}(\delta_{\alpha\beta} - \hat{\mathbf{Q}}_\alpha\hat{\mathbf{Q}}_\beta)\tilde{S}^{\alpha\beta}(\mathbf{Q},\omega). \tag{4}$$

In this expression $\tilde{S}^{\alpha\beta}(\mathbf{Q},\omega)$ is the convolution of the dynamic spin correlation function,[27]

$$S^{\alpha\beta}(\mathbf{Q},\omega) = \frac{1}{2\pi\hbar}\int dt e^{i\omega t}\frac{1}{N}\sum_{\mathbf{R}\mathbf{R}'}\langle S^\alpha_{\mathbf{R}}(t)S^\beta_{\mathbf{R}'}(0)\rangle \times e^{-i\mathbf{Q}\cdot(\mathbf{R}-\mathbf{R}')}, \tag{5}$$

with the normalized, instrumental resolution function in $\mathbf{Q}$-ω space.[28] Additional contributions to the count rate in the detector, however, arise from incoherent elastic nuclear scattering and inelastic scattering from phonons. These background contributions may be isolated by examining the T dependence of the scattering data. Magnetic neutron scattering from an isotropic one-dimensional magnet satisfies the total moment sum rule

$$3\int_\pi^{2\pi}\frac{d\tilde{q}}{\pi}\int \hbar\, d\omega\tilde{I}(\tilde{q},\omega) = \sum_\alpha \int_\pi^{2\pi}\frac{d\tilde{q}}{\pi}\int \hbar\, d\omega S^{\alpha\alpha}(\tilde{q},\omega) = S(S+1), \tag{6}$$

whereas inelastic nuclear scattering increases with temperature according to the Bose-Einstein thermal population factor $1 + n(\omega) = 1/[1 - \exp(-\beta\hbar\omega)]$. At sufficiently high T, scattering from phonons is therefore the dominant inelastic contribution to the intensity. At $T = 85$ K the integrated magnetic scattering cross section accounts for only 26% of the integrated inelastic intensity, and so we took data over our selected range of $\mathbf{Q}$ and ω at this temperature. As expected, these data were only weakly $\tilde{q}$ and ω dependent, and so to improve statistics we performed a moving average which effectively coarsened the resolution to $\delta\tilde{q} = 0.2$ and $\hbar\,\delta\omega = 0.4$. After appropriate scaling with the ω-dependent ratio of Bose-Einstein factors, this yielded the inelastic nuclear scattering background at $T = 1.8$ K, shown as open circles in Fig. 5.

Incoherent elastic nuclear scattering is approximately T independent for $T \ll \Theta_D$ and this allows us to derive its contribution to the detector count rate by comparing data at $T = 1.8$ and 85 K. To this end we used the following ansatz for the low-energy nuclear scattering intensity:

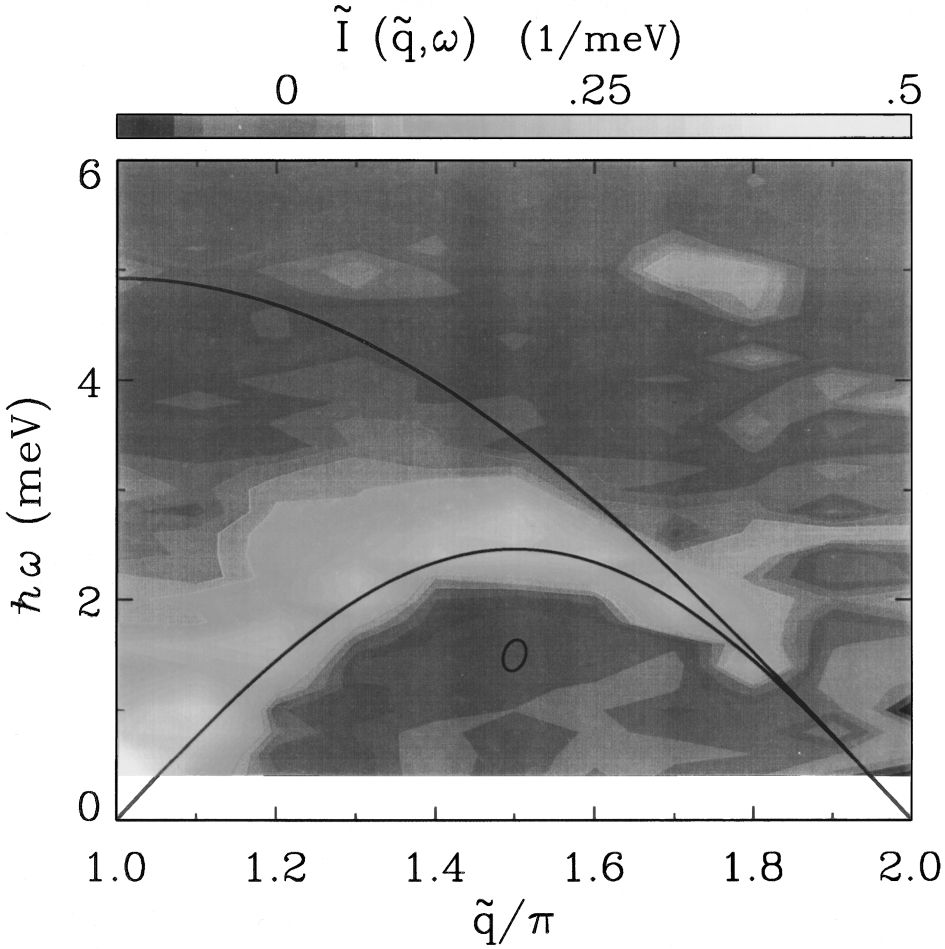

FIG. 6. Contour plot of background subtracted and normalized magnetic neutron scattering intensity from copper benzoate at $T = 1.8$ K. The ellipsoid is the half maximum contour of the instrumental resolution function. Solid lines are boundaries of the spinon continuum given by Eqs. (2) and (3) in the text with $J = 1.57$ meV.

$$I(\tilde{q},\omega)=f(\tilde{q})g(\omega)+C(\tilde{q})\frac{\omega}{1-e^{-\beta\hbar\omega}}, \tag{7}$$

where $g(\omega)$ is a sharply peaked function of ω normalized to 1 at $\omega=0$ that describes the elastic scattering profile and the second term accounts for the incoherent inelastic nuclear scattering. We extracted $g(\omega)$ by fitting $\tilde{q}$-integrated data with $\hbar\omega<\epsilon_1(\tilde{q})$ at $T = 1.8$ K and $T = 85$ K to the $\tilde{q}$ integral of this equation. Subsequent scaling by $f(\tilde{q})\approx I(\tilde{q},\omega=0)$ yielded an accurate measure of the ''wings'' of the elastic scattering profile, shown in Fig. 5 as open diamonds.

After subtracting these two background components we divided the data by the squared magnetic form factor[26] and normalized it by imposing the total moment sum rule of Eq. (6). The resulting magnetic intensity distribution $\tilde{I}(\tilde{q},\omega)$ is shown as a color contour map in Fig. 6. At first glance the data resemble inelastic scattering from a classical long range ordered antiferromagnet. The intensity is highest close to $\tilde{q}=\pi$ and $\hbar\omega=0$ and as $\tilde{q}$ varies through the Brillouin zone there is a ridge in $\tilde{q}$-ω space which approximately follows a sinusoidal dispersion relation. Closer examination of the data, however, reveals an important qualitative result: The asymmetric maximum in $\tilde{I}(\tilde{q},\omega)$ for $\tilde{q}\approx\pi$ is much broader than the half maximum resolution ellipse also shown in Fig. 6. From this observation it follows that $\tilde{I}(\tilde{q},\omega)$ *cannot* be accounted for by the discrete dispersion relation of conventional long-lived spin wave excitations. Instead, the data bear evidence of a continuum of excited states. The solid lines in Fig. 6 are the boundaries of the spinon continuum $\epsilon_1(\tilde{q})$ and $\epsilon_2(\tilde{q})$ [Eqs. (2) and (3)], calculated using the value $J=1.57$ meV, derived from our susceptibility measurements. Whereas the data are too noisy to identify an upper bound on the continuum, they do show clear evidence of a resolution-limited lower edge which follows $\epsilon_1(\tilde{q})$, the des Cloiseaux–Pearson lower bound on the energy of excited states with wave vector $\tilde{q}$ in the $S=1/2$ one-dimensional antiferromagnet.

Müller *et al.*[5,6] have derived an approximate model for the dynamic spin correlation function $S(\tilde{q},\omega)$ of the $S=1/2$ chain,

$$S^{\alpha\alpha}(\tilde{q},\omega)=\frac{1}{2\pi}\frac{A}{\sqrt{(\hbar\omega)^2-\epsilon_1^2(\tilde{q})}}\Theta(\hbar\omega-\epsilon_1(\tilde{q}))\times\Theta(\epsilon_2(\tilde{q})-\hbar\omega), \tag{8}$$

where $\Theta(x)$ is the step function. There are two parameters in this model, A and J. Taking the value $J=1.57$ meV obtained from our susceptibility measurements, we performed a simultaneous one-parameter fit of Eq. (4) convolved with the instrumental resolution function[28] to the entire data set represented in Fig. 6. The model provides a good fit to the data ($\chi^2=2.3$) for $A=1.2\pm0.2$. Not surprisingly, given that we normalized our data by imposing the total moment sum rule, this value of A is indistinguishable from the value $A\approx1.347$ for which Eq. (8) satisfies the same sum rule.[5]

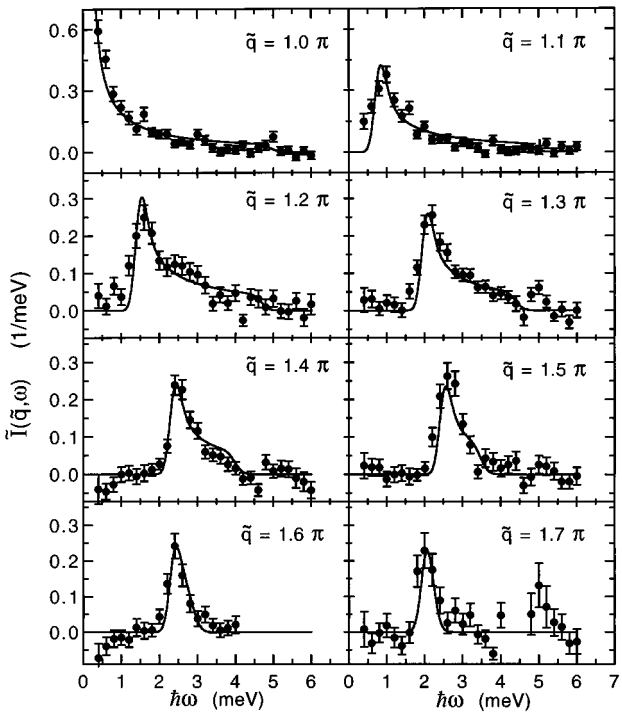

FIG. 7. Constant $\tilde{q}$ cuts through the magnetic neutron scattering data shown in Fig. 6. Solid lines are a one-parameter fit of the theory of Müller *et al.* (Refs. 5,6) to the entire data set.

Figure 7 provides a detailed comparison of model and data from which it is evident that our magnetic neutron scattering data from copper benzoate are very well accounted for by Eq. (8).

IV. SUMMARY AND CONCLUSION

Through high-field susceptibility measurements and inelastic neutron scattering we have shown that copper benzoate is a quasi-one-dimensional $S=1/2$ antiferromagnet with an exchange constant $J=1.57\pm0.01$ meV. Weak ferromagnetic behavior at low temperature and low magnetic field was carefully characterized, and we have determined that it is likely to result from spin canting in the three-dimensional antiferromagnetic state and has little consequence for $g\mu_B H/J>0.1$ or $\hbar\omega/J>0.25$. Although we could not grow large single crystals of the material, we have demonstrated the feasibility of combining large numbers of single crystals to form an oriented sample suitable for neutron scattering experiments. Using this sample we obtained a map of the dynamic spin correlation function $S(\tilde{q},\omega)$ at $k_BT/J=0.1$ for $\pi<\tilde{q}<2\pi$ and $0.25J<\hbar\omega<3.8J$. These data clearly show a bounded continuum of excited states as has been predicted for the one-dimensional $S=1/2$ antiferromagnet. The approximate expression for $S(\tilde{q},\omega)$ derived by Müller *et al.* for zero temperature adequately describes the data with an overall scale factor as the only adjustable parameter. The value of the exchange constant in copper benzoate, $J=1.57$ meV, renders this organic magnet an excellent system in which to study the field dependence of $S(\tilde{q},\omega)$ for the $S=1/2$ antiferromagnetic spin chain. First, as our experiments demonstrate, adequate energy resolution and sensitivity is obtained on conventional cold-neutron triple-axis spectrometers. Second, given a 10 T superconducting magnet it will be possible to achieve a reduced field $h=(g\mu_B H/J)=0.8$ which will bring the system deeply into the high-field phase where unusual incommensurate spin correlations have been predicted.[6,17] High-field inelastic neutron scattering experiments in copper benzoate to explore this phase are currently underway.

ACKNOWLEDGMENTS

We are grateful to Risø National Laboratory for their hospitality during the neutron scattering experiments, R. W. Erwin for assistance with cryogenics in an initial experiment at NIST, and C. Landee for helpful discussions. We thank R. Lindstrom and R. Paul of NIST for performing the Neutron Activation analysis. K.L. has been supported by a grant from the Danish Research Academy (Forskerakademiet). This work was supported in part by by the National Science Foundation through Grant Nos. DMR-9302065, DMR-9357518, and DMR-9453362. D.H.R. acknowledges support from the David and Lucile Packard Foundation. Acknowledgement is also made to the Donors of The Petroleum Research Fund, administered by the American Chemical Society, for partial support of this research.

*Also at National Institute of Standards and Technology, Gaithersburg, MD, 20899.
†Also at Risø National Laboratory, DK-4000 Roskilde, Denmark.

[1] H. Bethe, Z. Phys. **71**, 205 (1931); L. Hulthén, Ark. Mat. Astron. Fys. **26A**, No. 11 (1938).
[2] A. Luther and I. Peschel, Phys. Rev. B **12**, 3908 (1975).
[3] L. D. Faddeev and L. A. Takhtajan, Phys. Lett. **85A**, 375 (1981).
[4] J. des Cloizeaux and J. J. Pearson, Phys. Rev. **128**, 2131 (1962).
[5] G. Müller, H. Beck, and J. C. Bonner, Phys. Rev. Lett. **43**, 75 (1979).
[6] G. Müller, H. Thomas, H. Beck, and J. C. Bonner, Phys. Rev. B **24**, 1429 (1981).
[7] T. Yamada, Prog. Theor. Phys. Jpn. **41**, 880 (1969).
[8] P. C. Hohenberg and W. F. Brinkman, Phys. Rev. B **10**, 128 (1974).
[9] S. V. Meshkov, Phys. Rev. B **48**, 6167 (1993).
[10] J. Deisz, M. Jarell, and D. L. Cox, Phys. Rev. B **42** , 4869 (1990).
[11] Y. Endoh, G. Shirane, R. J. Birgenau, P. M. Richards, and S. L. Holt, Phys. Rev. Lett. **32**, 170 (1974).
[12] I. U. Heilmann, G. Shirane, Y. Endoh, R. J. Birgeneau, and S. L. Holt, Phys. Rev. B **18**, 3530 (1978).
[13] M. T. Hutchings, H. Ikeda, and J. M. Milne, J. Phys. C **12**, L739 (1979).
[14] S. K. Satija, J. D. Axe, G. Shirane, H. Yoshizawa, and K. Hirakawa, Phys. Rev. B **21**, 2001 (1980).
[15] S. E. Nagler, D. A. Tennant, R. A. Cowley, T. G. Perring, and S. K. Satija, Phys. Rev. B **44**, 12 361 (1991).
[16] D. A. Tennant, T. G. Perring, R. A. Cowley, and S. E. Nagler, Phys. Rev. Lett. **70**, 4003 (1993).
[17] N. Ishimura and H. Shiba, Prog. Theor. Phys. Jpn. **57**, 1862 (1977).
[18] J. P. Groen, T. O. Klassen, N. J. Poulis, G. Müller, H. Thomas,

and H. Beck, Phys. Rev. B **22**, 5369 (1980).
[19] H. J. Schulz, Phys. Rev. B **34**, 6372 (1986).
[20] M. Date, H. Yamazaki, M. Motokawa, and S. Tazawa, Suppl. Prog. Theor. Phys. **46**, 194 (1970).
[21] H. Koizumi, K. Osaki, and T. Watanabé, J. Phys. Soc. Jpn. **18**, 117 (1963).
[22] J. C. Bonner and M. E. Fisher, Phys. Rev. **135**, A640 (1964).
[23] K. Okuda, H. Hata, and M. Date, J. Phys. Soc. Jpn. **33**, 1574 (1972); K. Oshima, K. Okuda, and M. Date, *ibid.* **41**, 475 (1976); Y. Ajiro and M. Hamashima, *ibid.* **42**, 473 (1977); Y. Ajiro, Y. Nakajima, Y. Furukawa, and H. Kiriyama, *ibid.* **44**, 420 (1978); M. Hamashima and Y. Ajiro, *ibid.* **44**, 1743 (1978); K. Nagata and K. Okuda, *ibid.* **46**, 1726 (1979).
[24] K. Oshima, K. Okuda, and M. Date, J. Phys. Soc. Jpn. **44**, 757 (1978).
[25] H and D concentrations were determined by prompt γ-ray neutron activation analysis performed at the National Institute of Standards and Technology.
[26] A. J. Freeman and R. E. Watson, Acta Crystallogr. **14**, 231 (1961).
[27] We use the notation of S. W. Lovesey, *Theory of Neutron Scattering from Condensed Matter* (Clarendon Press, Oxford, 1984).
[28] N. D. Chesser and J. D. Axe, Acta Crystallogr. A **29**, 160 (1973).
[29] I. Dzyaloshinsky, J. Phys. Chem. Solids **4**, 241 (1958); T. Moriya, Phys. Rev. **117**, 635 (1960).
[30] H. A. Groenendijk, A. J. van Duyneveldt, and R. D. Willett, J. Magn. Magn. Mater. **15-18**, 1035 (1980).